On the effects of seasonality on soil water balance and plant growth

Xue Feng,[1] Giulia Vico,[1,2] and Amilcare Porporato[1,2]

Received 10 August 2011; revised 13 January 2012; accepted 30 March 2012; published 23 May 2012.

[1] The partitioning of rainfall into evapotranspiration, runoff, and deep infiltration in seasonally dry climates is influenced by strong temporal variability in rainfall and potential evapotranspiration at the intra-annual scale, which cannot be captured by conventional steady state water balance models. Guided by dimensional analysis and using simplified stochastic soil moisture models, we develop analytical expressions describing the annual partitioning of rainfall into evapotranspiration and deep percolation/runoff in seasonally dry, surface water dependent landscapes. We discuss the related changes to Budyko's curve under different seasonality scenarios, showing that an increase in seasonal rainfall and potential evapotranspiration variability as well as dry season length can lead to a decrease in the annual evapotranspiration ratio. In addition, our model shows that although increased soil water storage can compensate for the decrease in evapotranspiration due to climate seasonality, this effect is more marked in drier climates (higher annual dryness index) compared to wetter climates. Finally, the coupling of the soil moisture model to a minimalist plant growth model shows that in seasonally dry climates, a maximum in biomass is to be expected for a wet season of optimal length, for which the limitations imposed by both water availability and growth duration are at a minimum.

Citation: Feng, X., G. Vico, and A. Porporato (2012), On the effects of seasonality on soil water balance and plant growth, *Water Resour. Res.*, *48*, W05543, doi:10.1029/2011WR011263.

1. Introduction

[2] Evapotranspiration has long been recognized as the result of synergistic interactions between climate, soil, and vegetation [e.g., *Brutsaert*, 1982; *Rodriguez-Iturbe and Porporato*, 2004]. It is strongly influenced not only by the plant type and species composition at a site, but also by the overall economy of available water and energy. *Budyko* [1974] observed that under conditions of relative water abundance long-term evapotranspiration becomes limited by the potential evapotranspiration (PET), while in arid regions, where the energy supply is high, precipitation is the main constraint to evapotranspiration. In the former case, water supply exceeds demand, while in the latter case water supply is outstripped by the demand. On these premises *Budyko* [1974] proposed a semiempirical framework in which the ratio of mean annual evapotranspiration to rainfall (the evapotranspiration ratio) is related to a monotonically increasing function of the annual dryness index (D), defined as the ratio of mean annual PET to rainfall. Other studies have introduced similar functions, based either on empirical observations [*Pike*, 1964; *Choudhury*, 1999] or on boundary conditions mathematically imposed by water and energy balances [*Fu*, 1981; *Zhang et al.*, 2001, 2004; *Yang et al.*, 2008].

[3] The applicability of these water balance models is often limited by their implicit assumption of temporal steady state [*Porporato et al.*, 2004; *Donohue et al.*, 2007]. *Budyko and Zubenok* [1961] noted from empirical observations that basins characterized by the same mean annual dryness index can generate different amounts of runoff and that this variability is influenced by the seasonal patterns of precipitation and PET. For example, when the water and energy supplies are out of phase, observed mean annual evapotranspiration is lower than the amount predicted in the absence of seasonality, while it is higher when water and energy supplies are in phase. Furthermore, an annual rainfall amount concentrated in a few wet months can result in drastically different hydrological behavior and vegetation compared to the same amount spread evenly over the year. Thus, an increasing number of authors have come to recognize the need to resolve climatic inputs at a seasonal time scale [*Milly*, 1994a, 1994b; *Potter et al.*, 2005; *Hickel and Zhang*, 2006; *Gerrits et al.*, 2009]. In a modeling framework describing the long term balance of precipitation and evapotranspiration, *Milly* [1994a] introduced an index of seasonality as the normalized difference between the amplitudes of precipitation and PET, predicting decreasing annual evapotranspiration with stronger in-phase seasonality, in accordance with Budyko's observations. *Milly* [1994b] subsequently incorporated rainfall stochasticity as a Poisson process and described the dependence of the annual water partition on seven dimensionless parameters, including those that captured the plant-available soil water storage and the amplitude of seasonal variations in precipitation intensity, storm arrival rate (frequency), and PET.

[1]Department of Civil and Environmental Engineering, Duke University, Durham, North Carolina, USA.
[2]Nicholas School of the Environment and Earth Sciences, Duke University, Durham, North Carolina, USA.

0043-1397/12/2011WR011263

[4] In the absence of seasonality, dimensional analysis highlights the importance of the storage index (γ)—soil water storage capacity relative to mean rainfall depth—in addition to Budyko's dryness index, in defining the rainfall partition at the annual level [*Milly*, 1993; *Porporato et al.*, 2004]. Empirical observations further reveal the complex role played by soil water storage in rainfall-dominated seasonal climates. To distinguish between seasonal rainfall regimes that are in or out of phase with PET, *Potter et al.* [2005] extended the stochastic model developed by *Milly* [1994b] by adding a phase shift term to the sinusoidal functions previously used for precipitation intensity, frequency, and PET. The numerical solutions predicted that, for cases with the same mean annual dryness index, the evapotranspiration ratio for catchments with summer-dominant rainfall regimes (in phase) was higher than catchments with winter-dominant rainfall (out of phase). However, this was found to be surprisingly in contrast with observed data. *Potter et al.* [2005] attributed this discrepancy to infiltration-excess runoff, which was not explicitly modeled and which may have effectively lowered the soil water storage during periods of intense rainfall in the summer. Using a larger set of catchment data and decomposing evapotranspiration into climate- and storage-controlled components, *Hickel and Zhang* [2006] corroborated the evidence that the average effective storage is indeed smaller in summer-dominant rainfall catchments (due likely to high runoff ratios during intense rain events in the summer, as already suggested by *Potter et al.* [2005]), and the climate-controlled component of evapotranspiration (which bypassed the effect of soil water storage) is higher for summer-dominant catchments, as predicted by most previous models. These studies show that the storage index can compensate for seasonal rainfall variability by mediating the portion of rainfall that is actually available for plant uptake, something also shown by *Gerrits et al.* [2009].

[5] The importance of seasonality and the need to account for it have been observed in the context of other ecohydrological traits, such as the distribution of plant communities in North America [*Stephenson*, 1990] and the fraction of coexisting annual and perennial grasses in Mediterranean ecosystems [*Clary*, 2008]. Thus, the strong link known to exist between evapotranspiration and plant growth naturally suggests that climatic conditions that result in variations in evapotranspiration may necessitate concomitant adaptations in growth strategies [*Stephenson*, 1998; *Viola et al.*, 2008].

[6] In this study we present an idealized framework based on dimensional analysis, to study the seasonality of rainfall and PET in terms of both intensity and duration. We couple this framework with a process-based model of stochastic soil moisture balance [*Porporato et al.*, 2004; *Rodriguez-Iturbe and Porporato*, 2004] and derive analytical solutions for the mean annual water balance. As in previous works on the subject [*Reggiani et al.*, 2000; *Yokoo et al.*, 2008], the parameters of our model are chosen to describe Budyko's curve and its modifications. Our approach however also offers causal explanations for the resulting curves as it clearly ties physical processes to model structure, allowing us to specifically investigate the importance of rainfall and PET seasonality as well as the relative durations of the wet and dry seasons under different soil water storage capacities in water-controlled seasonal climates. Finally, the implication of rainfall variability on biomass accumulation are explored using a simple growth model that is directly linked to the soil moisture model.

2. Stochastic and Seasonal Variability of Soil Moisture

[7] At daily scale, assuming negligible horizontal redistribution via topographic effects, soil moisture at a point is recharged through intermittent rainfall pulses of random depths, and depleted through evapotranspiration, drainage, and runoff. In what follows, we focus on the vertically averaged, plant available "effective" soil moisture x defined as $\frac{s-s_w}{s_1-s_w}$, where s is the relative soil moisture, and s_w and s_1 correspond, respectively, to the plant wilting point and the effective saturation level, above which soil water is assumed to be immediately lost to drainage or runoff. The range of x—between 0 and 1—brackets the upper and lower limits of soil moisture available for plant uptake. With the above assumptions, the effective soil moisture balance, vertically averaged over the rooting zone, is [*Rodriguez-Iturbe and Porporato*, 2004]

$$w_0 \frac{dx(t)}{dt} = R(t) - ET[x(t)] - LQ[x(t), t], \tag{1}$$

where $w_0 = (s_1 - s_w)nZ_r$ is the maximum plant-available soil water storage volume per unit ground area, n (dimensionless) is the vertically averaged soil porosity, and Z_r (e.g., cm) is the average rooting depth. The rate of change in the total volume of plant-available soil moisture $\left(w_0 \frac{dx(t)}{dt}\right)$ is governed by the rate of precipitation R (e.g., cm day^{-1}), evapotranspiration ET (e.g., cm day^{-1}), and leakage/runoff LQ (e.g., cm day^{-1}).

[8] Rainfall and PET, the latter controlling the evapotranspiration rate ET in (1), fluctuate at different time scales and are characterized by intraseasonal, seasonal, and interannual variability. Moreover, the unpredictable nature of rainfall calls for a stochastic framework in the analysis of the soil moisture balance [*Rodriguez-Iturbe and Porporato*, 2004; *Katul et al.*, 2007]. We will thus assume that the observed hydroclimatic processes are one realization of a stochastic ensemble given by the underlying random process. For seasonal climates we will assume that embedded within this random variability is a deterministic seasonal component repeating itself with yearly period T^{yr} and divided into two distinct seasons, a wet season followed by a dry season, $T^{\mathrm{yr}} = T^w + T^d$. The origin of time t is set at the beginning of a generic wet season.

[9] The following notations will be used: the ensemble average of a generic variable $u \in [u_{\min}, u_{\max}]$ with probability density function $p(u,t)$ at a specific instant of time is denoted by brackets, i.e., $\langle u(t) \rangle = \int_{u_{\min}}^{u_{\max}} up(u,t)\,\mathrm{d}u$; the temporal average over a time period T (e.g., over an entire year or a season) is denoted by overbars, defined as $\overline{u}^T(t_0, T) = \frac{1}{T}\int_{t_0}^{t_0+T} u(t)\,\mathrm{d}t$, where t_0 is the beginning time of interest. Note that $\overline{u}^T(t_0, T)$ is still a random variable; it is only when the ensemble average of the time average is taken, $\langle \overline{u}^T(t_0, T) \rangle$, that it becomes deterministic. Moreover, if the process is stationary, the long-term time average

$\overline{u}^{\infty} = \lim_{T\to\infty} \frac{1}{T}\int_{-T/2}^{+T/2} u(t)\,dt$ becomes independent of t_0 and is the same as the ensemble average, i.e., $\overline{u}^{\infty} = \langle u \rangle$; in this case, the process is said to be ergodic. In what follows we will be interested in the ensemble averages of annual, wet-season, and dry-season averages, i.e., $\langle \overline{u}^{T^{yr}} \rangle$, $\langle \overline{u}^{T^{w}} \rangle$, and $\langle \overline{u}^{T^{d}} \rangle$, indicated for short as $\langle \overline{u}^{yr} \rangle$, $\langle \overline{u}^{w} \rangle$, and $\langle \overline{u}^{d} \rangle$, respectively.

3. Dimensional Analysis of the Annual Water Balance

[10] We now use dimensional analysis to derive seasonal parameters governing the annual water balance. A key assumption in the dimensional analysis that follows is that only two parameters are needed to describe the instantaneous evapotranspiration: potential evapotranspiration (ET_{max}) and plant available effective soil moisture (x). Since x is in turn governed by equation (1), it is necessary to include w_0, R, and LQ for a more complete characterization of ET, although we will waive LQ from the list of independent governing parameters when considering long-term averages since LQ is complementary to ET in that case. We make a further assumption that the rainfall regime at a given time can be described simply by the mean depth α and the frequency λ of storm events. Note that this formulation does not take in account the role of groundwater in vegetation dynamics and assumes that the plant characteristics s_1 and s_w are already known.

3.1. General Formulation With No Seasonality

[11] In the absence of seasonality, the water balance is assumed to be at stochastic steady state and therefore ergodic, i.e., $\langle \overline{ET}^{yr} \rangle = \overline{ET}^{yr}$. According to the assumptions outlined at the beginning of the section, a general equation for the annual average evapotranspiration $\langle \overline{ET}^{yr} \rangle$ can be written as

$$\langle \overline{ET}^{yr} \rangle = f(ET_{max}, \alpha, \lambda, w_0). \tag{2}$$

[12] The Buckingham-Pi theorem with five dimensional parameters and two primary dimensions—length (e.g., cm) and time (e.g., day)—provides $5 - 2 = 3$ independent Π groups (see, e.g., *Barenblatt* [1996]). Selecting α (e.g., cm) and λ (e.g., day^{-1}) as the parameters that cover all the primary dimensions, the following dimensionless Π groups can be formed:

$$\Pi_1 = \phi(\Pi_2, \Pi_3), \tag{3}$$

where $\Pi_1 = \frac{\langle \overline{ET}^{yr} \rangle}{\alpha\lambda}$, $\Pi_2 = \frac{ET_{max}}{\alpha\lambda}$, and $\Pi_3 = \frac{w_0}{\alpha}$. By substituting the original parameters into functional form (3), a more meaningful relationship emerges, and the annual water balance in steady state becomes a function of Budyko's dryness index ($D = \Pi_2$) and the storage index ($\gamma = \Pi_3$),

$$\frac{\langle \overline{ET}^{yr} \rangle}{\langle \overline{R}^{yr} \rangle} = \phi(D, \gamma), \tag{4}$$

where $\frac{\langle \overline{ET}^{yr} \rangle}{\langle \overline{R}^{yr} \rangle} = \frac{\langle \overline{ET}^{yr} \rangle}{\alpha\lambda}$, $D = \frac{ET_{max}}{\alpha\lambda}$, and $\gamma = \frac{w_0}{\alpha}$.

[13] We note that the selection of the dimensionally independent governing parameters α and λ is arbitrary; in this case, the resulting functional forms reproduce Budyko's water balance relationship. If we instead select ET_{max} and w_0, then the functional relationship becomes $\frac{\langle \overline{ET}^{yr} \rangle}{ET_{max}} = \Phi\left(\gamma^{-1}, \frac{\lambda w_0}{ET_{max}}\right)$.

3.2. Dimensional Analysis With the Inclusion of Seasonality

[14] We now follow the same approach in the case where mean annual climatic conditions are no longer constant. We divide the year into a wet and a dry season, assuming that together they encapsulate the most essential features of seasonal variability. Both seasons are now characterized by their own set of climatic and soil-plant parameters, initial soil moisture conditions, and lengths. The mean evapotranspiration over each season takes the following forms:

$$\begin{aligned} \langle \overline{ET}^{w} \rangle &= f_w(ET^w_{max}, \alpha^w, \lambda^w, w_0^w, x_0^w, T^w), \\ \langle \overline{ET}^{d} \rangle &= f_d(ET^d_{max}, \alpha^d, \lambda^d, w_0^d, x_0^d, T^d). \end{aligned} \tag{5}$$

The annual mean evapotranspiration and rainfall are now determined from the time weighed contributions from both seasons,

$$\langle \overline{ET}^{yr} \rangle = \frac{\langle \overline{ET}^{w} \rangle T^w + \langle \overline{ET}^{d} \rangle T^d}{T^w + T^d}, \quad \langle \overline{R}^{yr} \rangle = \frac{\langle \overline{R}^{w} \rangle T^w + \langle \overline{R}^{d} \rangle T^d}{T^w + T^d}. \tag{6}$$

Combining equations (5) and (6) with the governing parameters from both seasons, and noting that the initial soil moisture conditions depend on the parameters of the previous season, the annually averaged evapotranspiration can be written as

$$\langle \overline{ET}^{yr} \rangle = f_s(ET^w_{max}, ET^d_{max}, \alpha^w, \alpha^d, \lambda^w, \lambda^d, w_0^w, w_0^d, T^w, T^d). \tag{7}$$

In order to simplify the analysis, we assume that the maximum plant available soil water storage capacity remains constant across seasons, $w_0 = w_0^w = w_0^d$, i.e., plant rooting depth and ability to capture soil water remains unaltered. We further assume that rainfall frequency (λ) is the dominant driver of rainfall variability and thus set the mean rainfall depth constant across seasons, i.e., $\alpha = \alpha^w = \alpha^d$. Selecting the wet season as the reference state, we use α and λ^w as the two parameters accounting for all primary dimensions and normalize the remaining parameters using Buckingham-Pi theorem to obtain the following functional form:

$$\frac{\langle \overline{ET}^{yr} \rangle}{\alpha\lambda^w} = \phi_s^*(\Pi_2, \Pi_2^*, \Pi_3, \Pi_r, \Pi_t, \Pi_t^*), \tag{8}$$

where $\Pi_2 = \frac{ET^w_{max}}{\alpha\lambda^w}$, $\Pi_2^* = \frac{ET^d_{max}}{\alpha\lambda^w}$, $\Pi_3 = \frac{w_0}{\alpha}$, $\Pi_r = \frac{\lambda^d}{\lambda^w}$, $\Pi_t = \lambda^w T^w$, and $\Pi_t^* = \lambda^w T^d$. Note that Π_2 and Π_3 are, respectively, the dryness index for the wet season D^w and the storage index γ found in (4). Of the other dimensionless groups, some combine parameters from the two seasons (e.g., Π_2^* and Π_t^*),

a fact stressed by the use of the superscript $*$, while others have more complex physical meanings $\left(\text{e.g., } \frac{\langle \overline{ET}^{yr} \rangle}{\alpha \lambda^w}\right)$. By multiplying several dimensionless groups together, we can combine them into more intuitive forms amenable to physical interpretation, without altering the overall functional dependence. Using $\langle \overline{R}^w \rangle = \alpha \lambda^w$, $\langle \overline{R}^d \rangle = \alpha \lambda^d$, and equation (6), equation (8) can be expressed as a function of the mean annual water balance $\frac{\langle \overline{ET}^{yr} \rangle}{\langle \overline{R}^{yr} \rangle}$ without introducing additional parameters. Likewise, the other dimensionless groups can be reorganized to give

$$\frac{\langle \overline{ET}^{yr} \rangle}{\langle \overline{R}^{yr} \rangle} = \phi_s(D^w, \gamma, \rho, \tau, \epsilon, \beta^d), \tag{9}$$

where $D^w = \frac{ET^w_{max}}{\alpha \lambda^w}$, $\gamma = \frac{w_0}{\alpha}$, $\rho = \frac{\lambda^d}{\lambda^w}$, $\tau = \frac{T^d}{T^w}$, $\epsilon = \frac{ET^d_{max}}{ET^w_{max}}$, and $\beta^d = \frac{ET^d_{max} T^d}{w_0}$. We will refer to this formulation throughout the rest of our developments. D^w is the dryness index in the reference (wet) season, γ is the storage index, ρ is the ratio of seasonal rainfall frequencies, τ is the ratio of seasonal durations, ϵ is the ratio of seasonal PET, and β^d is the dry season evaporative index, or the PET over the entire dry season normalized by the soil water storage capacity. The four dimensionless groups that appear in addition to D^w and γ are all associated with measures of seasonality. These dimensionless groups can be broadly adopted to analyze a variety of seasonal climates, provided that these climates can be idealized as the alternation of a dry and a wet season. Explicit forms of the function ϕ_s will be obtained in section 5. For subsequent use we also define the mean annual dryness index as

$$D^{yr} = \frac{ET^w_{max} T^w + ET^d_{max} T^d}{\alpha \lambda^w T^w + \alpha \lambda^d T^d} = D^w \frac{1 + \epsilon\tau}{1 + \rho\tau}. \tag{10}$$

4. Classification of Seasonal Hydroclimatic Regions

[15] The previously introduced seasonality parameters can be used to quantitatively characterize rainfall dominated seasonal climates. We follow the widely used Köppen-Geiger classification system [*Peel et al.*, 2007; *Lydolph*, 1985], focusing on climates with a pronounced dry season, especially tropical savanna (Aw), tropical monsoon (Am), and Mediterranean (Csa, Csb) climates.

[16] The tropical savanna climate, known also as the tropical wet-and-dry climate, is found at latitudes roughly between 5° to 20° [*Critchfield*, 1974]. Areas characterized by this climate type include western Central America, northwestern South America, interior Brazil, south-central and eastern Africa, Madagascar, India, Southeast Asia, and northern Australia. Due to the influence of equatorial and tropical air masses and high year-round net radiation, temperatures are high throughout the year (the coolest month averages 18°C or higher), and seasonal variation in temperature is low. The precipitation regime, on the other hand, is marked by a stark seasonal contrast. In the equatorial regions the dry season is short, but at higher latitudes the dry season becomes longer and the PET may exceed precipitation year round.

[17] Likewise, the tropical monsoon climate is found at low latitudes and has elevated temperature throughout the year. Its rainfall regime is comparable to the tropical savanna climates, characterized by a distinct and sustained dry season with low rainfall (albeit slightly higher than the driest monthly precipitation mark line set for tropical savanna climates). However, its annual total rainfall is much higher, resembling more the tropical rain forest climate (typically over 1500 mm) [*Critchfield*, 1974]. As a result, the contrast between the wet and the dry season may be even more drastic; typically, the dry months may receive less than 1/10 the rainfall of the wettest months.

[18] The Mediterranean climates are found at latitudes between 30° to 45° on the western continental margins, including in the Mediterranean basin, California, Chile, the southern tip of Africa, and southwestern Australia. They are classified based on their temperature variability (warmest month above 10°C and coldest month above 0°C) as well as their precipitation variability (the dry months receiving less than 1/3 of the precipitation typical of the wet months [*Lydolph*, 1985]). A chief feature of the Mediterranean climates is the dominance of the subtropical high air masses that result in hot, dry summers and cool, wet winters. Annual rainfall totals between 350 and 900 mm, with most of it falling during the cold winter season. The dry summers may last typically between five and six months.

[19] These main features of the above climates can be summarized using the dimensionless groups defined in section 3.2. The duration of the dry season for tropical savanna and monsoon climates can be more variable compared to that of Mediterranean climates, but it is around 6 months, corresponding to $\tau \approx 1$. PET is mainly driven by solar radiation and air temperature. Hence, the seasonal ratio in PET, or ϵ, hovers around 1 in tropical climates, where temperature and solar radiation do not significantly change throughout the year. On the other hand, in Mediterranean climates characterized by a hot summer and cool winter, ϵ is more variable (often ranging between 2 and 3). With respect to rainfall, Mediterranean and tropical savanna climates are typically characterized by comparable annual totals, yet the contrast between the wet and the dry season rainfall for tropical savannas is more pronounced. Although the rainfall in monsoon and tropical savannas may have similar seasonal variability, the larger rainfall totals typical of the monsoon regions results in a less intense dry season compared to the tropical savanna climates. The typical range of seasonal parameters for seasonally dry climates is summarized in Table 1.

5. Stochastic Models

[20] We use stochastic soil moisture models to link to the dimensionless groups in section 3 and obtain explicit

Table 1. Typical Range of Seasonal Parameters for Seasonally Dry Climates[a]

Climate Types	$\langle \overline{R}^{yr} \rangle$ (mm yr^{-1})	ET^d_{max} (cm day^{-1})	$\rho = \frac{\lambda^d}{\lambda^w}$	$\epsilon = \frac{ET^d_{max}}{ET^w_{max}}$	$\tau = \frac{T^d}{T^w}$
Tropical savanna	400–1500	0.35–0.70	10	1	0.7–1.4
Monsoon	>1500	0.35–0.70	10	1	0.7–1.4
Mediterranean	350–900	0.30–0.60	3	2–3	0.7–1.4

[a]Note: $\langle \overline{R}^{yr} \rangle$ is the average rainfall rate over a year. ET^d_{max} is variable according to plant functional types; the values shown are typical for trees.

forms for the annual water balance (ϕ_s in equation (9)). Within each season, rainfall is idealized as a marked Poisson process, with the distribution of the times between precipitation events drawn from an exponential distribution of mean $1/\lambda^s$, different for each season (the superscript s stands either for w in the wet season or d in the dry season), and the depth of rainfall drawn independently from an exponential distribution of mean α [*Rodriguez-Iturbe et al.*, 1999]. Accordingly, the effective soil moisture is a random variable with probability density function $p^s(x,t)$. The temporal evolution of the time dependent ensemble mean of soil moisture $\langle x^s(t)\rangle$ can be obtained from the macroscopic equation [*Laio et al.*, 2002; *Rodriguez-Iturbe and Porporato*, 2004]

$$\frac{\mathrm{d}\langle x^s(t)\rangle}{\mathrm{d}t} = \frac{\lambda^s}{\gamma} - \int_0^1 \frac{ET^s(u)}{w_0} p^s(u,t)\,\mathrm{d}u - \frac{\lambda^s}{\gamma}\int_0^1 e^{-\gamma(1-u)} p^s(u,t)\,\mathrm{d}u. \tag{11}$$

We will assume that the process has been started at $t \to -\infty$ and that $t = 0$ corresponds to the beginning of a generic wet season. Clearly the initial conditions of (11) are linked to those of (1). The terms on the right hand side in (11) are the ensemble averages of rainfall input and soil moisture losses normalized by the storage capacity, i.e.,

$$\frac{\lambda^s}{\gamma} = \frac{\langle R^s(t)\rangle}{w_0}, \tag{12}$$

$$\int_0^1 \frac{ET^s(u)}{w_0} p^s(u,t)\,\mathrm{d}u = \frac{\langle ET^s(x)\rangle}{w_0}, \tag{13}$$

$$\frac{\lambda^s}{\gamma}\int_0^1 e^{-\gamma(1-u)} p^s(u,t)\,\mathrm{d}u = \frac{\langle LQ^s(x,t)\rangle}{w_0}. \tag{14}$$

With a simple assumption of a linear dependence of $ET(x)$ on x, from 0 at $x = 0$ to $ET^s_{\max}$ (depending on the season) at $x = 1$ [*Porporato et al.*, 2004], equation (15) can be further simplified to

$$\int_0^1 \frac{ET^s(u)}{w_0} p^s(u,t)\,\mathrm{d}u = \frac{ET^s_{\max}}{w_0}\int_0^1 u p^s(u,t)\,\mathrm{d}u = \frac{ET^s_{\max}}{w_0}\langle x^s(t)\rangle. \tag{15}$$

On the other hand, the leakage and runoff term cannot be approximated easily. We apply two treatments of this term, one using a minimalist approach that leads to simple expressions, and another that uses a linear approximation of the $\langle LQ(x,t)\rangle$ term (the linear LQ model) that can more accurately describes the soil water balance when the storage index γ is very high or low.

[21] For the minimalist model, soil moisture is assumed to instantaneously reach stochastic steady state during the wet season and decay without leakage or runoff during the dry season (see Appendix A for a more detailed exposition). Using equations (6), (15), and corresponding solutions for $\langle x^s(t)\rangle$, the mean annual water balance can be recast as

$$\frac{\langle \overline{ET}^{\mathrm{yr}}\rangle}{\langle \overline{R}^{\mathrm{yr}}\rangle} = \frac{1}{1+\rho\tau}\left\{G^w + \rho\tau\left[1 - \frac{1}{\beta^d}\left(1 - G^w\frac{\epsilon}{\rho}\right)(1 - e^{-\beta^d})\right]\right\}, \tag{16}$$

where G^w is the fraction of evapotranspiration in the wet season

$$G^w = \frac{\langle \overline{ET}^w\rangle}{\langle \overline{R}^w\rangle} = 1 - D^w\frac{\gamma^{\frac{\gamma}{D^w}-1}e^{-\gamma}}{\Gamma\left(\frac{\gamma}{D^w}\right) - \Gamma\left(\frac{\gamma}{D^w},\gamma\right)}, \tag{17}$$

and $\Gamma(\cdot)$ is the gamma function and $\Gamma(\cdot,\cdot)$ is the incomplete gamma function [*Abramowitz and Stegun*, 1964; *Porporato et al.*, 2004].

[22] For the linear LQ model, $\langle LQ(x,t)\rangle$ is linearized by imposing a deterministic value at the beginning of each season and a long term value consistent with the stochastic steady state condition, as explained in Appendix B. Altogether, the water balance for the linear LQ model can be written as

$$\frac{\langle \overline{ET}^{\mathrm{yr}}\rangle}{\langle \overline{R}^{\mathrm{yr}}\rangle} = \frac{1}{1+\rho\tau}(\Omega^w + \rho\tau\Omega^d), \tag{18}$$

where

$$\Omega^w = \langle x^w\rangle_{ss} D^w + \frac{D^{w2}(x_0^w - \langle x^w\rangle_{ss})^2}{\beta^w[x_0^w D^w - 1 + \exp(-\gamma(1-x_0^w))]} \times \left[1 - \exp\left(-\beta^w\frac{x_0^w D^w - 1 + \exp(-\gamma(1-x_0^w))}{D^w(x_0^w - \langle x^w\rangle_{ss})}\right)\right], \tag{19}$$

$$\Omega^d = \langle x^d\rangle_{ss} D^d + \frac{D^{d2}(x_0^d - \langle x^d\rangle_{ss})^2}{\beta^d[x_0^d D^d - 1 + \exp(-\gamma(1-x_0^d))]} \times \left[1 - \exp\left(-\beta^d\frac{x_0^d D^d - 1 + \exp(-\gamma(1-x_0^d))}{D^d(x_0^d - \langle x^d\rangle_{ss})}\right)\right] \tag{20}$$

are the evapotranspiration fraction during the wet and the dry season, respectively, with their corresponding soil moisture value x_0^s at the beginning of each season and $\langle x^s\rangle_{ss}$ at stochastic steady state (see Appendix B), $D^d = \frac{D^w\epsilon}{\rho}$, and $\beta^w = \frac{\epsilon\tau}{\beta^d}$.

[23] The temporal evolution of the mean available soil moisture $\langle x(t)\rangle$ obtained by the minimalist and linear LQ model are compared to one another and with the result of a numerical simulation in Figure 1a. The difference in $\langle x(t)\rangle$ from the minimalist and numerical simulation is most relevant for very shallow soils due to the non-negligible leakage/runoff at the beginning of the dry season and for very deep soils due to the slow recharge at the beginning of the wet season (Figure 1a). The restrictions related to the minimalist model is further discussed in Appendix A. The linear LQ model, on the other hand, is able to approximate the temporal evolution of soil moisture more closely to the numerical simulation for a wider range of parameters, and thus will be used in the rest of analyses for mean annual water balance $\frac{\langle \overline{ET}^{\mathrm{yr}}\rangle}{\langle \overline{R}^{\mathrm{yr}}\rangle}$. The parametric curves for $\frac{\langle \overline{ET}^{\mathrm{yr}}\rangle}{\langle \overline{R}^{\mathrm{yr}}\rangle}$ are plotted as a function of the annual dryness index D^{yr} (equation (10)), generated by both analytical models in Figure 1b. As expected, the minimalist model performs well around intermediate dryness index values, but with extremely high or low soil water storage index or high

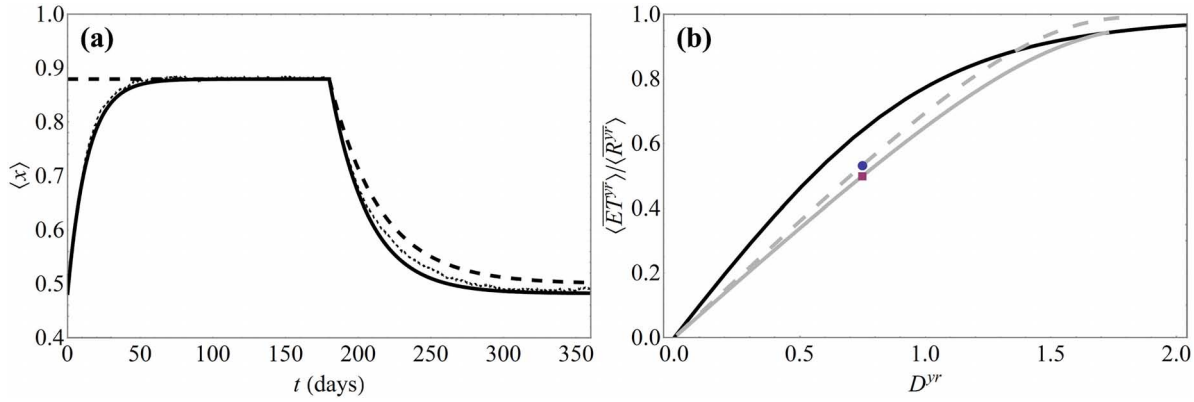

Figure 1. Comparison of the minimalist and the linear *LQ* model applied to the seasonal soil water balance. (a) Temporal evolution of mean soil moisture $\langle x(t) \rangle$ using numerical simulations (dotted lines), the *LQ* model (solid lines), and the minimalist model (dashed lines), with $\gamma = 10.4$, $ET^d_{\max} = ET^w_{\max} = 0.45$ cm d^{-1}, $w_0 = 15.6$ cm, $\alpha = 1.5$ cm, $\lambda^w = 0.45$ d^{-1}, $\lambda^d = 0.15$ d^{-1}, and $\tau = 1$. (b) Corresponding soil water balance represented by the aseasonal Budyko's curve for $\gamma = 10.4$ (black solid line) and seasonal curves using the minimalist model (gray dashed line) and the linear *LQ* model (gray solid line). Other parameters are as in Figure 1a except for variations in λ^w. The soil water balance for the realizations in Figure 1a are represented by a single point in Figure 1b (minimalist model, circle; linear *LQ* model, square).

dryness index, it tends to generate ratios of $\langle \overline{ET}^{yr} \rangle$ to $\langle \overline{R}^{yr} \rangle$ above 1. This a direct consequence of the overestimation in evapotranspiration due to the higher-than-realistic soil moisture obtained with the minimalist model already observed with the specific choices of parameters in Figure 1a.

6. Effect of Seasonality on Budyko's Curve

[24] In the following analysis we employ the results from the linear *LQ* model to explore the effects of climate seasonality on the annual average soil water balance by means of Budyko-like curves.

6.1. Role of Rainfall Variability and Dry Season Length (ρ and τ)

[25] Figure 2a shows the shift in the Budyko's curve from the aseasonal case ($T^d = 0$; solid black line) to the seasonal case with increasing dry season length (the particular case of a 6 month dry season, i.e., $\tau = 1$, is represented by the solid gray line). We consider two alternative constraints on rainfall as the dry season length is increased: (1) total annual rainfall is kept constant by redistributing rainfall from the dry to the wet season, i.e., increasing λ^w while keeping λ^d constant (resulting in a decrease in the ratio of rainfall frequencies ρ; dashed lines) and (2) λ^w, λ^d, and hence ρ are kept constant by decreasing total annual rainfall (dotted lines). As the dry season length (and thus τ) is increased, a single point on the aseasonal Budyko's curve (black solid line) will shift to the right, following one of two trajectories associated the previously described rainfall constraints, with different rates of change for both the annual dryness index D^{yr} and evapotranspiration ratio $\frac{\langle \overline{ET}^{yr} \rangle}{\langle \overline{R}^{yr} \rangle}$. Points at equal intervals along the Budyko's curve are used to show these relative rates of increase for the two cases. For a fixed τ, all the endpoints of these trajectories fall onto the same line (solid gray line for $\tau = 1$). As such, the seasonal curve is independent of the method used to generate it: a single point on the Budyko's curve may trace out different trajectories, but their endpoints for a given τ will always coincide on the same curve regardless of the path they followed from Budyko's.

[26] An important consequence of the results shown in Figure 2a is that, at a given annual dryness index, the overall effect of increasing the dry season length, with or without a concomitant increase in seasonal rainfall variability (i.e., ρ), is a decrease in the evapotranspiration ratio. This effect is especially accentuated around the intermediate dryness indices, where the difference between aseasonal and seasonal evapotranspiration is greatest.

6.2. Role of Variability in Potential Evapotranspiration (ϵ)

[27] Tropical ($ET^w_{\max} \approx ET^d_{\max}$; $\epsilon \approx 1$) and Mediterranean climates ($ET^w_{\max} < ET^d_{\max}$; $\epsilon > 1$) can be compared by modifying the potential evapotranspiration ratio ϵ. By assuming that the dry-season PET is not significantly different between tropical and Mediterranean climates, we focus our analyses on the effect of a decrease in $ET^w_{\max}$ while $ET^d_{\max}$ is kept constant (resulting in ϵ increasing to values greater than 1). As discussed in section 6.1, an increase in dry season length and/or seasonal rainfall variability decreases the evapotranspiration ratio at a given annual dryness index compared to when the same total annual rainfall is distributed evenly throughout the year. As apparent in Figure 2b, this effect is further enhanced in Mediterranean climates ($\epsilon > 1$) relative to tropical climates ($\epsilon \approx 1$). Due to rainfall and PET being out of phase in Mediterranean climates, the evapotranspiration ratio further decreases as rainfall accumulate in the soil during the cold wet season without being used by plants, enhancing losses to runoff and deep percolation. In other words, an increase in ϵ decreases $\frac{\langle \overline{ET}^{yr} \rangle}{\langle \overline{R}^{yr} \rangle}$ beyond the limit already imposed by the length of the dry season (τ) and/or degree of rainfall seasonality (ρ).

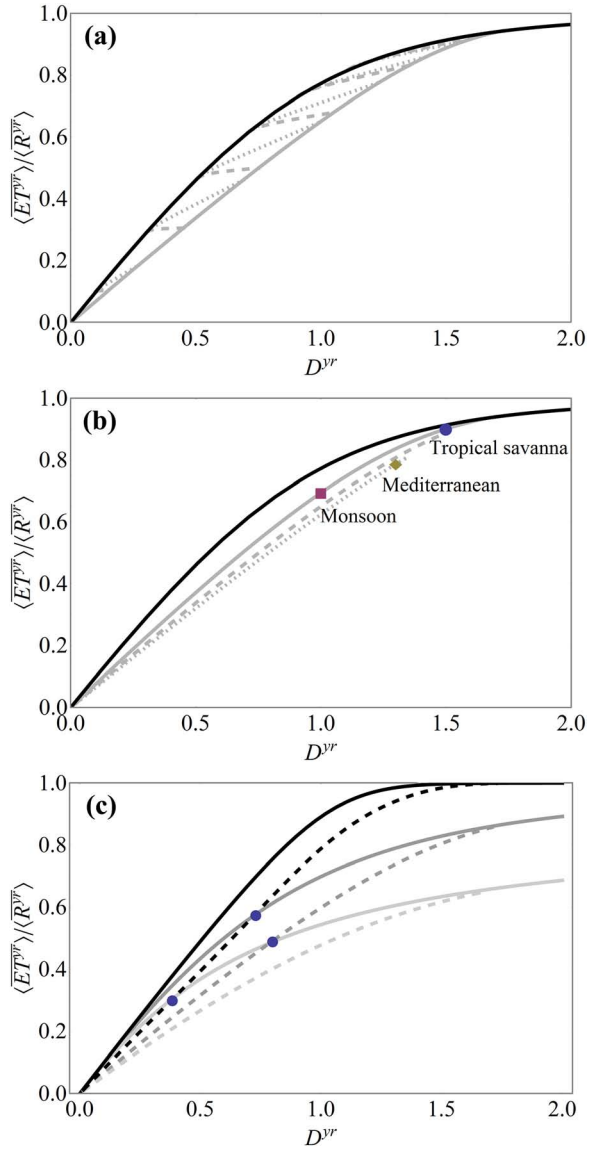

Figure 2. The effects of seasonality parameters on Budyko's curve. (a) Effect of dry season length with T^d increasing from 0 (black line) to $T^d = 180$ days (i.e., 6 month long dry season; $\tau = 1$, gray solid line), with constant total annual rainfall (dashed lines) and constant rainfall frequency ρ (dotted lines). (b) Effect of seasonal ratio of PET, $\epsilon = \frac{ET^d_{\max}}{ET^w_{\max}}$:$\epsilon = 1$ (gray solid line), $\epsilon = 2$ (gray dashed line), and $\epsilon = 3$ (gray dotted line). Symbols represent typical values from each climate type. (c) Effect of the storage index $\gamma = \frac{w_0}{\alpha}$:$\gamma = 2$ (light gray), 5.5 (gray), and 50 (black) with and without seasonality (dashed and solid lines, respectively). Dots denote the intersections between a dashed and a solid line. All results are obtained with the linear *LQ* model. Unless otherwise specified, $\tau = 1$, $\epsilon = 2$, and $\gamma = 10.4$. Dry season parameters are always set to $\alpha = 1.5$ cm, $\lambda^d = 0.15$ d^{-1}, and $ET^d_{\max} = 0.45$ cm d^{-1}.

6.3. Role of the Soil Water Storage Index (γ)

[28] The storage index $\gamma = \frac{w_0}{\alpha}$ is an explicit function of several plant and soil parameters—soil porosity (n), plant rooting depth (Z_r), plant wilting point (s_w), and maximum soil water retention point (s_1)—and how they compare to average rainfall depth α. In the absence of seasonality, higher γ implies a larger proportion of rainfall stored and retained in the soil rather than lost as runoff or deep percolation (either due to higher soil water storage capacity or shallow rainfall events that tend not to saturate the soil). Thus, larger γ in aseasonal climates results in a larger percentage of rainfall used for evapotranspiration, represented by an upward shift in Budyko's curve ([*Porporato et al.*, 2004]; Figure 2c, gray to black solid lines).

[29] The role of the storage index γ is more complex in seasonal climates, where it also represents the inertia with which soil moisture changes between seasons. For a fixed α, soil and plant parameters ensuring a higher storage index not only results in a higher steady state soil moisture value but also in a slower rate of change in response to climatic inputs, especially apparent at the junctions between the wet and dry seasons. Because larger inertia associated with larger γ results in a more moderate range of soil moisture values year round, the decrease in leakage/runoff (due to soil moisture values farther from saturation) combined with higher storage can yield higher evapotranspiration ratios even in seasonal climates (Figure 2c, dashed lines).

[30] A comparison of seasonal and aseasonal Budyko's curves also suggests that the impact of seasonality and storage index on the evapotranspiration ratio depends on the dryness index of the climate under consideration. Toward drier end of the curves, deeper roots in seasonal climates can result in higher evapotranspiration compared to shallower roots in aseasonal climates at a given dryness index. This is likely due to the added water storage capacity provided by deeper roots. Toward wetter climates, however, deeper roots in seasonal climates eventually lose their advantage. In fact, wetter seasonal climates are associated with a tremendous concentration of rainfall during the wet season, which causes soil moisture to quickly reach stochastic steady state; the higher losses to leakage/runoff that ensue can effectively lower the evapotranspiration ratio to an extent that cannot be compensated by an increase in storage. These trade-offs are apparent in the locations of the intersections between aseasonal and seasonal curves of different storage indices (marked by dots in Figure 2c). The most important consequence is that the decrease in evapotranspiration due to climate seasonality can be balanced by higher storage indices, e.g., by developing deeper roots; this in turn can be more easily accomplished in drier climates than in wetter climates (Figure 2c). A caveat of this analysis is the assumption that typical rooting depths and climate conditions are independent. Nevertheless, roots are generally deeper in arid and seasonally dry climates [*Schenk and Jackson*, 2002a]; this correlation may serve to offset the large differences in the evapotranspiration ratio between different storage indices in drier climates.

7. Plant Response to Seasonality

[31] In this section we apply the results presented in the previous sections to a simple model of plant growth, and use them to extrapolate the effects of altered seasonality at the ecosystem level. Because of the strong coupling between transpiration and CO_2 assimilation, evapotranspiration has

strong connections to plant growth [*Rosenzweig*, 1968; *Major*, 1967] and morphology [*Stephenson*, 1990]. Thus the effect of seasonality on plants follows inevitably from its effect on soil moisture and evapotranspiration. For Mediterranean climates, on the basis of vegetation surveys, *Clary* [2008] has already established a correlation between the seasonality of rainfall (in particular the relative strength of the summer drought) and the species composition, independent of other factors. In semideciduous tropical forests of southeastern Brazil, *Oliveira-Filho and Fontes* [2000] found the floristic composition to be most strongly correlated with proxies of increasing rainfall seasonality. In the following analyses we explore the consequences for plant biomass of altering the season lengths while maintaining a constant total annual rainfall, effectively concentrating rainfall into the wet season as the dry season length is increased. The two end-member scenarios encountered by the plants are a mild water stress imposed over a prolonged period of time (i.e., a long "wet" season and short dry season, resulting in soil moistures mostly under mild to moderate stress), and extreme stress during a long dry season with relatively high soil moisture during a short wet season.

[32] To assess the effect of rainfall seasonality on the temporal evolution of plant biomass B and to explore the possible existence of an optimal duration of the wet season for a given total annual rainfall, we couple the previous stochastic soil moisture model to a minimalist model of plant growth. Because of the simplifications inherent in the soil moisture model, the obtained results are applicable to the case where vegetation is unable to access additional water stores, such as groundwater, and is fully dependent on rainfall and soil water availability to meet its evapotranspiration demands. In order to isolate the effect of rainfall seasonality from other drivers of growth (e.g., temperature in Mediterranean climates), we focus our analysis on tropical climates where the wet season coincides with the growing season. Defining B as the maximum attainable biomass at a single time point under ideal conditions, encompassing also the biomass lost to litter production, root secretion, and consumers, the relative growth rate $\frac{1}{B}\frac{dB}{dt}$ can be written as

$$\frac{1}{B}\frac{dB}{dt} = k(A - R), \tag{21}$$

where A is the gross assimilation rate, R is the respiration rate, and k is the product of the specific leaf area (leaf area per leaf mass) and leaf mass ratio (leaf mass per unit plant biomass).

[33] To proceed quantitatively, we assume that assimilation and respiration rates are driven by the ensemble mean effective soil moisture $\langle x(t)\rangle$ derived in the previous seasonality model. Although plant response depends on the full distribution of soil moisture (as well as its temporal structure), this approximation allows us to capture the main effect of water stress without excessively complicating the analytical treatment. Following *Daly et al.* [2004], we assume analogous drought responses in all climates and adopt a piecewise-linear dependence of gross assimilation rate on the mean ensemble effective soil moisture, with a maximum assimilation rate of $A_{\max}$ under well watered conditions ($\langle x\rangle \geq x^*$) and falling to zero under intense stress ($\langle x\rangle = 0$). The soil moisture threshold x^* represents a mean soil moisture level below which plants reduce growth due to water stress [*Hsiao*, 1973; *Porporato et al.*, 2001; *Larcher*, 2003]. This pattern is supported by empirical observations across Mediterranean [*Gimenez*, 1992; *Galmés et al.*, 2007a; *Peguero-Pina et al.*, 2009; *Shane et al.*, 2010] and semiarid tropical species [*Gindaba et al.*, 2004; *Muthuri et al.*, 2009]. Consistent with the general decline observed across many species in assimilation-to-respiration ratio with increasing water stress, we further assume respiration decreases from a fraction of the assimilation $R_{\max}$ (anywhere between 20% and 70% of $A_{\max}$ depending on the plant type and climate zone), to a minimum, nonzero value $R_{\min}$ [*Larcher*, 2003; *Flexas et al.*, 2005, 2006; *Ribas-Carbó et al.*, 2005; *Galmés et al.*, 2007b]. We introduce another soil moisture threshold $x_{cr} < x^*$ at which net assimilation is zero, i.e., $A(x_{cr}) = R(x_{cr})$. No feedback of B on soil moisture, specific leaf area, or leaf mass ratio is considered.

[34] The temporal evolution of plant biomass can be obtained by solving equation (21), with $\langle x(t)\rangle$ encapsulating the effects of seasonality in rainfall. For a given total annual rainfall, biomass B increases at the maximum rate during the wet season; such rate will be $A_{\max} - R_{\max}$ when $\langle x\rangle$ is above x^*. After the end of the wet season, as the mean soil moisture drops, the relative growth rate gradually diminishes along with net assimilation $A(\langle x\rangle) - R(\langle x\rangle)$ until the threshold x_{cr} is reached (Figure 3a). The biomass at $\langle x(t)\rangle = x_{\mathrm{cr}}$ corresponds to the peak biomass for the year. A further decrease in soil moisture below x_{cr} results in negative net assimilation, and theoretically to a decrease in B. Since plant response at this stage varies widely, from drought dormancy to deciduousness and even death, our minimalist model cannot capture plant adaptations beyond this point. We will instead focus on the seasonal peak in biomass B_p (reached at $\langle x(t)\rangle = x_{\mathrm{cr}}$) for a given ratio of dry season to wet season length, τ. For a short dry season, annual rainfall is redistributed over a long wet season during which the soil moisture is relatively low; thus the peak biomass is reached via slow but steady growth, limited by water availability (Figure 3a, light gray line). Conversely, for a long dry season, rainfall is concentrated over the short wet season, resulting in transiently high soil moisture. The absence of water limitations results in a rapid biomass growth (at maximum rate), which however does not last long because of the subsequent onset of the dry season. Thus, the peak seasonal biomass depends on the relative lengths of the seasons, with a maximum occurring under an optimal wet season of intermediate length, in which the total rainfall is distributed in such a way that allows for plants to take advantage of abundant water during most of the growing season. A longer dry season ($\tau > \tau_{\mathrm{opt}}$) means that plant growth is limited by time, while a longer wet season ($\tau < \tau_{\mathrm{opt}}$) means that plant growth is limited by water availability. With the choice of parameters in Figure 3a (i.e., for an annual rainfall of 450 mm), such maximum in peak biomass is attained for $T^w = 210$ days, i.e., $\tau_{\mathrm{opt}} \approx 0.7$.

[35] The achievable peak in B clearly depends as well on the total annual rainfall. This is made evident by plotting the peak seasonal biomass B_p (a single point for each line in Figure 3a) for different amounts of total annual rainfall

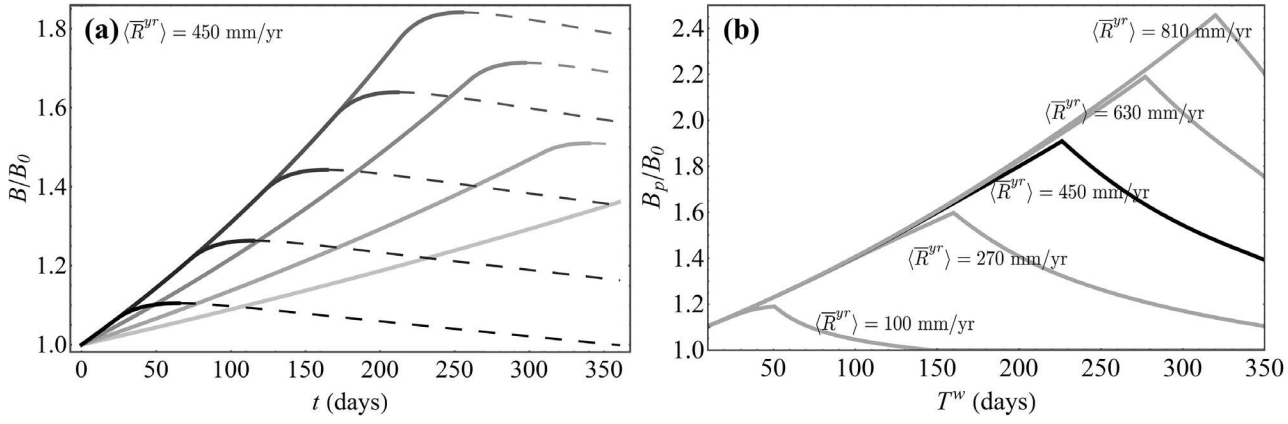

Figure 3. Effect of rainfall seasonality on biomass accumulation. (a) Temporal evolution of biomass B for different lengths of the wet season, for mean annual rainfall rate $\langle \overline{R}^{yr} \rangle = 450$ mm yr^{-1}. Each line corresponds to a wet season length from $T^w = 10$ (black line) to $T^w = 360$ (light gray line) in 50 day intervals; the maximum biomass is attained for $T^w = 210$ days (mid gray line). Dashed lines are used to indicate theoretical changes in biomass beyond the peak point. Other soil and climatic parameters are $\alpha = 0.50$ cm , $\lambda^d = 0.05$ d^{-1}, $\lambda^w = 0.25$ d^{-1}, $ET^d_{\max} = ET^w_{\max} = 0.50$ cm d^{-1}, $w_0 = 10$ cm, and $x^* = 0.55$. Plant parameters refer to *Panicum virgatum* (switchgrass) [*Shipley*, 2002]: net assimilation rate $A_{\text{net}} = 0.0018$ g cm^{-2} day^{-1} ($A_{\max} = A_{\text{net}}/0.4$, $R_{\max} = 0.6A_{\max}$, $R_{\min} = 0.1A_{\max}$), leaf mass ratio = 0.46, and specific leaf area = 325 cm^2 g^{-1}. Initial biomass B_0 is set to 100 g. (b) Maximum attainable (peak) seasonal biomass B_p as function of wet season length T^w for different annual rainfall rates. All the other parameters are as in Figure 3a. The black line has the same annual rainfall rate used in Figure 3a and, when superimposed to Figure 3a, would connect the peak biomass points.

and wet season length (Figure 3b). Overall, peak biomass is low when the dry season becomes too long and the wet season rainfall is too concentrated, or when the total annual rainfall is low. For a given total annual rainfall, the maximum peak biomass is obtained at an intermediate ratio of T^d/T^w, showing the existence of an optimal duration of the wet season. Increasing total annual rainfall relieves the restriction on water availability during the wet season and, as can be seen in Figure 3b, allows for a longer period of maximum growth (and thus a decrease in τ_{opt}).

8. Conclusions

[36] In this study we use dimensional analysis to develop a generalized framework for evaluating the role of seasonal climatic variability on soil moisture and mean annual evapotranspiration in rainfall dominated, surface water dependent systems. Assuming that the year consists of a distinct sequence of a wet and a dry season, we define a set of dimensionless quantities describing the seasonality of rainfall occurrence and plant activity. By combining this framework with a stochastic soil moisture balance model, the mean annual soil water balance can be analytically obtained. Generally, a stronger seasonality (e.g., due to longer dry seasons or stronger variability in rainfall or PET between the two seasons) results in more runoff and percolation losses and lower evapotranspiration ratio.

[37] Our model shows that the influences of seasonal climate and soil water storage on evapotranspiration observed by *Hickel and Zhang* [2006] and *Gerrits et al.* [2009] can also be explained through the compensatory role played by soil water storage for changes in annual evapotranspiration resulting from rainfall seasonality. In seasonal climates, the effect of an increase in plant-available soil water storage capacity (chiefly driven by rooting depth) depends on the dryness index at the site (Figure 2c). In drier seasonal climates, the increase in total annual evapotranspiration achieved through deeper roots and more soil water storage easily overtakes the decrease due to rainfall seasonality. On the other hand, in wetter seasonal climates, the concentration of rainfall in the wet season saturates the soil despite increased storage, resulting in an overall decrease in evapotranspiration ratio. Care should be taken when comparing the evapotranspiration ratios across soil water storage indices because this model assumes rooting depths act independently from climate conditions (even though deeper roots are generally found in more arid and seasonal climates [*Schenk and Jackson*, 2002a, 2002b]) and across plant types (when rooting depth can sometimes correlate with other plant characteristics such as stomatal conductance, leaf area index, and PET).

[38] When coupled to a simple plant biomass model, our framework shows the existence of an optimal wet season length given constant annual rainfall (related to τ_{opt}, see Figure 3) that conciliates the trade-off between water-limited growth rate and growing season length, in the absence of additional rainfall-independent water stores available to vegetation. The existence of such optimal wet season length could be tested by comparing biomass indices (e.g., NDVI) from regions with the same annual rainfall but differing in their seasonal distributions. The simultaneous influence of annual rainfall totals and seasonality has already been demonstrated in India, where humid forest types are differentiated from each other based on their dry

season lengths, while the driest ecosystems such as thornbush savannas and deserts were more defined by their total annual rainfall [*Walter*, 1971].

[39] The present analysis uses an idealized representation of seasonality. In particular, the temporal variability of rainfall and PET are captured at the seasonal scale only, using two constant levels to represent the relative magnitudes of the climatic drivers across seasons. The assumption in this model of a fixed duration of the seasons as well as their fixed start and finish times have implications for plant phenology and its ensuing effects on evapotranspiration. One extension could be the inclusion of temporal variability of hydroclimatic signals at different scales, from intra-annual to interannual fluctuations, as well as a finer resolution of their relative timing (beyond being either in phase or out of phase) and uncertain arrivals. Other controls such as vegetation dynamic can also prove revealing, by incorporating feedbacks from plant biomass to soil moisture, soil nutrient dynamics, plant resource allocation, and life strategies. Altogether, these additions will lend further insights into the roles of variable hydroclimatic forcing and soil-plant conditions in seasonally dry ecosystems.

Appendix A: The Minimalist Model

[40] A minimalist approach to the description of the soil water balance is to assume that soil moisture is instantaneously brought to a stochastic steady state at the beginning of the wet season. Thus for the wet season the stochastic steady state solution for the soil moisture model of *Porporato et al.* [2004] is adopted, resulting in the following average effective soil moisture:

$$\langle x^w \rangle_{ss} = \frac{1}{D^w} - \frac{\gamma^{\frac{\gamma}{D^w}-1}}{\Gamma\left(\frac{\gamma}{D^w}\right) - \Gamma\left(\frac{\gamma}{D^w}, \gamma\right)} e^{-\gamma}, \tag{A1}$$

where $\Gamma(\cdot)$ is the gamma function and $\Gamma(\cdot,\cdot)$ is the incomplete gamma function [*Abramowitz and Stegun*, 1964].

[41] Conversely, during the dry season, the soil moisture cannot realistically be considered at stochastic steady state. Nevertheless, the analytical description can be simplified by noticing that the infrequent rainfall events typical of the dry season result in infrequent runoff and deep percolation events. At a first approximation, it is thus possible to neglect the upper bound on x without introducing significant errors (see, e.g., *Viola et al.* [2008]). Thus, setting $\langle LQ(x,t)\rangle$ to zero in equation (14), the temporal evolution of the ensemble average $\langle x(t)\rangle$ can be obtained by solving the macroscopic equation (11) with the initial condition $\langle x^d(t = T^w)\rangle = \langle x^w\rangle_{ss}$ (equation (A1)), to obtain for $T^w \le t < T^{\mathrm{yr}}$

$$\langle x^d(t)\rangle = \frac{1}{D^d} + \left[\langle x^w\rangle_{ss} - \frac{1}{D^d}\right] \exp\left(-\left(\frac{ET^d_{\max}}{w_0}\right)t\right), \tag{A2}$$

where $D^d = \frac{D^w \epsilon}{\rho}$ is the dryness index in the dry season. This ensemble mean soil moisture decays exponentially from the mean value found at the end of the wet season.

[42] With the above approximations, the time averaged evapotranspiration during a single season can be calculated using $\langle \overline{ET}^s \rangle = \frac{1}{T^s}\int_{t_0}^{t_0+T^s} ET^s_{\max}\langle x^s(t)\rangle \, \mathrm{d}u$ (where $t_0 = 0$ for the wet season and $t_0 = T^w$ for the dry season), and with equations (6), (15), and the dimensionless groups defined in section 3, the annual water balance can be recast into equation (16).

[43] Figure 1a shows the evolution of soil moisture generated by the minimalist model (dashed line) compared to that generated by a numerical simulation using the same parameters (dotted line). The minimalist seasonal model provides a good approximation for soil moisture in water-limited ecosystems where leakage and runoff are negligible compared to other terms during the dry season and soil moisture quickly reaches stochastic steady state after the beginning of the wet season. In presence of a marked dry season, with PET high relative to rainfall, leakage and runoff tends to be negligible when the ratio of effective soil water storage to rainfall depth γ is relatively large or the frequency of rainfall λ^d is relatively small. However, during the wet season, the same conditions (large γ, small λ^w) increase the inertia of soil moisture response to rainfall forcing, resulting in a substantial time lag between the start of the rainy season and when the soil moisture reaches stochastic steady state (see Figure 1a). Consequently, the minimalist seasonal model can occasionally lead to unsuitable overestimates of soil moisture, especially when γ is large. In summary, the minimalist seasonal model cannot be applied to climates lacking a prominent dry season, including tropical rain forest, humid subtropical, and maritime climates, or when the inertia of the soil moisture process (as defined by γ) is high and the stochastic steady state is not readily reached at the beginning of the wet season.

Appendix B: The Linear *LQ* Model

[44] To improve the description of the mean water balance when the minimalist model is not a good approximation, we introduce a linear approximation for the leakage and runoff ensemble averages in equation (14). Since $\langle LQ(x,t)\rangle$ is state dependent and requires the full determination of the time-dependent soil moisture pdf, it is extremely difficult to find it a priori. A satisfactory approximation, however, can be obtained noting that $\langle LQ(x,t)\rangle$ is known in two special cases: if the soil moisture pdf is deterministic (i.e., the pdf of soil moisture is concentrated at a point) and at stochastic steady state.

[45] Assuming that at the beginning of each season the soil moisture pdf is concentrated around a soil moisture level x_0^s, where the superscript s stands for either season, the pdf is a Dirac delta function $\delta(x - x_0^s)$, which, when substituted into the runoff term (14), gives

$$\frac{\langle LQ^s\rangle_0}{w_0} = \frac{\lambda^s}{\gamma} e^{-\gamma(1-x_0^s)}. \tag{B1}$$

Moreover, the mean soil moisture will be x_0^s at the beginning of the season.

[46] Furthermore, the macroscopic equation (11) can be linearized by linearizing both the ET and the LQ terms, resulting in exponential dependence in time of $\langle x^s(t)\rangle$ toward the stochastic steady state value $\langle x^s\rangle_{ss}$. Using

$\langle ET^s \rangle_{ss} = ET^s_{\max} \langle x \rangle^s_{ss}$, the dryness index D^s, and equation (A1) for $\langle x^s \rangle_{ss}$, we obtain for each seasonal partitioning

$$\langle LQ^s \rangle_{ss} = \langle R^s \rangle - \langle ET^s \rangle_{ss} = \alpha \lambda^s \frac{D^s \gamma^{\frac{\gamma}{D^s}-1}}{\Gamma\left(\frac{\gamma}{D^w}\right) - \Gamma\left(\frac{\gamma}{D^w}, \gamma\right)} e^{-\gamma}. \quad \text{(B2)}$$

[47] Combining these approximations, the linearization of $\langle LQ^s(x,t) \rangle$ for each season is then given by

$$\langle LQ^s(x,t) \rangle = \frac{\langle LQ^s \rangle_{ss} - \langle LQ^s \rangle_0}{\langle x^s \rangle_{ss} - x^s_0} (\langle x(t) \rangle - x^s_0) + \langle LQ^s \rangle_0. \quad \text{(B3)}$$

Substituting equation (B3) into (14) and solving the macroscopic equation (11), we obtain the temporal evolution of the soil moisture ensemble during one season

$$\langle x^s(t) \rangle = \langle x^s \rangle_{ss} + [x^s_0 - \langle x^s \rangle_{ss}] \exp\left(-\left(\frac{ET^s_{\max} + \theta^s}{w_0} \right) t \right), \quad \text{(B4)}$$

where the effect of leakage is introduced in the exponential decay coefficient $\theta^s = \frac{\langle LQ^s \rangle_{ss} - \langle LQ^s \rangle_0}{\langle x^s \rangle_{ss} - x^s_0}$ (using (B1) and (B2)) and x^s_0 must be found by the continuity condition between the two seasons by imposing $x^d_0 = \langle x^w(T^w) \rangle$ and $x^w_0 = \langle x^d(T^d) \rangle$. As is the case for the minimalist model, once the ensemble soil moisture evolution for each season is found, the time averaged evapotranspiration can be calculated as $\langle \overline{ET}^s \rangle = \frac{1}{T^s} \int_{t_0}^{t_0+T^s} ET^s_{\max} \langle x^s(t) \rangle \, \mathrm{d}u$, and the annual water balance (18) can then be derived from equations (6) and (15) and the dimensionless groups.

[48] **Acknowledgments.** This work was partially funded by the National Science Foundation through grant NSF-CBET-1033467 and by the U.S. Department of Energy through the Office of Biological and Environmental Research (BER) Terrestrial Ecosystem Science (TES) Program (DE-SC0006967). The authors would also like to thank Edoardo Daly, Ignacio Rodriguez-Iturbe, and two anonymous reviewers for providing helpful suggestions for improving the manuscript.

References

Abramowitz, M., and I. A. Stegun (1964), *Handbook of Mathematical Functions*, Dover Publications, New York.

Barenblatt, G. I. (1996), *Scaling, Self-Similarity, and Intermediate Asymtotics*, Cambridge University Press, Cambridge.

Brutsaert, W. F. (1982), *Evaporation Into the Atmosphere*, Kluwer Academic Publishers, Dordrecht, Holland.

Budyko, M. I. (1974), *Climate and Life*, Academic Press, New York.

Budyko, M. I., and L. I. Zubenok (1961), Determination of evaporation from the land surface (in Russian), *Izv. Akad. Nauk SSSR, Ser. Geogr.*, *6*, 3–17.

Choudhury, B. J. (1999), Evaluation of an empirical equation for annual evaporation using field observations and results from a biophysical model, *J. Hydrol.*, *216*, 99–110.

Clary, J. (2008), Rainfall seasonality determines annual/perennial grass balance in vegetation of Mediterranean Iberian, *Plant Ecol.*, *195*, 13–20.

Critchfield, H. J. (1974), *General Climatology*, 3rd ed., Prentice-Hall, Englewood Cliffs, NJ.

Daly, E., A. Porporato, and I. Rodriguez-Iturbe (2004), Coupled dynamics of photosynthesis, transpiration, and soil water balance. Part II: Stochastic analysis and ecohydrological significance, *J. Hydrometeor.*, *5*, 559–566.

Donohue, R. J., M. L. Roderick, and T. R. McVicar (2007), On the importance of including vegetation dynamics in Budyko's hydrological model, *Hydrol. Earth Syst. Sci.*, *11*, 983–995.

Flexas, J., J. Galmés, M. Ribas-Carbó, and H. Medrano (2005), The effects of water stress in plant respiration, in *Advances in Photosynthesis and Respiration 18. Plant Respiration: From Cell to Ecosystem*, edited by H. Lambers and M. Ribas-Carbó, pp. 85–94, Kluwer Academic, Dordrecht.

Flexas, J., J. Bota, J. Galmés, H. Medrano, and M. Ribas-Carbó (2006), Keeping a positive carbon balance under adverse conditions: Responses of photosynthesis and respiration to water stress, *Physiol. Plantarum*, *127*, 343–352.

Fu, B. P. (1981), On the calculation of the evaporation from land surface (in Chinese), *Sci. Atmos. Sin.*, *5*, 23–31.

Galmés, J., H. Medrano, and J. Flexas (2007a), Photosynthetic limitations in response to water stress and recovery in Mediterranean plants with different growth forms, *New Phytol.*, *175*(1), 81–93.

Galmés, J., H. Medrano, and J. Flexas (2007b), Response of leaf respiration to water stress in Mediterranean species with different growth forms, *J. Arid Environ.*, *68*(2), 206–222.

Gerrits, A. M. J., H. H. G. Savenije, E. J. M. Veling, and L. Pfister (2009), Analytical derivation of the Budyko curve based on rainfall characteristics and a simple evaporation model, *Water Resour. Res.*, *45*, W04403, doi:10.1029/2008WR007308.

Gimenez, C., V. J. Mitchell, and D. W. Lawlor (1992), Regulation of photosynthetic rate of two sunflower hybrids under water stress, *Plant Physiol.*, *98*(2), 516–524.

Gindaba, J., A. Rozanov, and L. Negash (2004), Response of seedlings of two Eucalyptus and three deciduous tree species from Ethiopia to severe water stress, *For. Ecol. Manage.*, *201*(1), 119–129.

Hickel, K., and L. Zhang (2006), Estimating the impact of rainfall seasonality on mean annual water balance using a top-down approach, *J. Hydrol.*, *331*(3–4), 409–424.

Hsiao, T. C. (1973), Plant responses to water stress, *Ann. Rev. Plant Physiol.*, *24*, 519–570.

Katul, G., A. Porporato, and R. Oren (2007), Stochastic dynamics of plant-water interactions, *Annu. Rev. Ecol. Evol. S.*, *38*, 767–791.

Laio, F., A. Porporato, L. Ridolfi, and I. Rodriguez-Iturbe (2002), On the seasonal dynamics of mean soil moisture, *J. Geophys. Res.*, *107*(D15), 4272, doi:10.1029/2001JD001252.

Larcher, W. (2003), *Physiological Plant Ecology: Ecophysiology and Stress Physiology of Functional Groups*, 4th ed., Springer Verlag, Berlin.

Lydolph, P. E. (1985), *The Climate of the Earth*, Rowman & Allanheld, Totowa, New Jersey.

Major, J. (1967), Potential evapotranspiration and plant distributions in western states with emphasis on California, *Ground Level Climatology*, edited by R. H. Shaw, Publ. 86, pp. 93–126, American Association for the Advancement of Science, Washington, D.C.

Milly, P. C. D. (1993), An analytical solution of the stochastic storage problem applicable to soil water, *Water Resour. Res.*, *29*(11), 3755–3758.

Milly, P. C. D. (1994a), Climate, interseasonal storage of soil water, and the annual water balance, *Adv. Water Resour.*, *17*(1–2), 19–24.

Milly, P. C. D. (1994b), Climate, soil water storage, and the average annual water balance, *Water Resour. Res.*, *30*(7), 2143–2156.

Muthuri, C. W., C. K. Ong, J. Craigon, B. M. Mati, V. W. Ngumi, and C. R. Black (2009), Gas exchange and water use efficiency of trees and maize in agroforestry systems in semi-arid Kenya, *Agric. Ecosyst. Environ.*, *129*(4), 497–507.

Oliveira-Filho, A. T. and M. A. L. Fontes (2000), Patterns of floristic differentiation among Atlantic forests in southeastern Brazil and the influence of climate, *Biotropica*, *32*(4b), 793–810.

Peel, M. C., B. L. Finlayson, and T. A. McMahon (2007), Updated world map of the Koppen-Geiger climate classification, *Hydrol. Earth Syst. Sci.*, *11*(5), 1633–1644.

Peguero-Pina, J. J., D. Sancho-Knapik, F. Morales, J. Flexas, and E. Gil-Pelegrin (2009), Differential photosynthetic performance and photoprotection mechanisms of three Mediterranean evergreen oaks under severe drought stress, *Funct. Plant Biol.*, *36*(5), 453–462.

Pike, J. G. (1964), The estimation of annual runoff from meteorological data in a tropical climate, *J. Hydrol.*, *2*(2), 116–123.

Porporato, A., F. Laio, L. Ridolfi, and I. Rodriguez-Iturbe (2001), Plants in water-controlled ecosystems: Active role in hydrologic processes and response to water stress. III. Vegetation water stress, *Adv. Water Resour.*, *24*(7), 725–744.

Porporato, A., E. Daly, and I. Rodriguez-Iturbe (2004), Soil water balance and ecosystem response to climate change, *Am. Nat.*, *164*(5), 625–632.

Potter, N. J., L. Zhang, P. C. D. Milly, T. A. McMahon, and A. J. Jakeman (2005), Effects of rainfall seasonality and soil moisture capacity on mean annual water balance for Australian catchments, *Water Resour. Res.*, *41*, W06007, doi:10.1029/2004WR003697.

Reggiani, P., M. Sivapalan, and S. M. Hassanizadeh (2000), Conservation equations governing hillslope responses: Exploring the physical basis of water balance, *Water Resour. Res.*, *36*(7), 1845–1863.

Ribas-Carbó, M., N. T. Taylor, L. Giles, S. Busquests, P. M. Finnegan, D. A. Day, H. Lambers, H. Medrano, J. A. Berry, and J. Flexas (2005), Effects of water stress on respiration in soybean leaves, *Plant Physiol.*, *139*, 466–473.

Rodriguez-Iturbe, I., and A. Porporato (2004), *Ecohydrology of Water-Controlled Ecosystems: Soil Moisture and Plant Dynamics*, Cambridge University Press, Cambridge.

Rodriguez-Iturbe, I., A. Porporato, L. Ridolfi, V. Isham, and D. R. Cox (1999), Probabilistic modelling of water balance at a point: The role of climate, soil and vegetation, *Proc. R. Soc. London A*, *455*, 3789–3805.

Rosenzweig, M. L. (1968), Net primary productivity of terrestrial communities: Prediction from climatological data, *Am. Nat.*, *102*(923), 67–74.

Schenk, H. J., and R. B. Jackson (2002a), The global biogeography of roots, *Ecol. Monogr.*, *72*(3), 311–328.

Schenk, H. J., and R. B. Jackson (2002b), Rooting depths, lateral root spreads and below-ground/above-ground allometries of plants in water-limited ecosystems, *J. Ecol.*, *90*(3), 480–494.

Shane, M. W., M. E. McCully, M. J. Canny, J. S. Pate, C. Huang, H. Ngo, and H. Lambers (2010), Seasonal water relations of Lyginia barbata (Southern rush) in relation to root xylem development and summer dormancy of root apices, *New Phytol.*, *185*(4), 1025–1037.

Shipley, B. (2002), Trade-offs between net assimilation rate and specific leaf area in determining relative growth rate: Relationship with daily irradiance, *Funct. Ecol.*, *16*(5), 682–689.

Stephenson, N. L. (1990), Climatic control of vegetation distribution: The role of the water balance, *Am. Nat.*, *135*(5), 649–670.

Stephenson, N. L. (1998), Actual evapotranspiration and deficit: Biologically meaningful correlates of vegetation distribution across spatial scales, *J. Biogeogr.*, *25*(5), 855–870.

Viola, F., E. Daly, G. Vico, M. Cannarozzo, and A. Porporato (2008), Transient soil-moisture dynamics and climate change in Mediterranean ecosystems, *Water Resour. Res.*, *44*, W11412, doi:10.1029/2007WR006371.

Walter, H. (1971), *Ecology of Tropical and Subtropical Vegetation*, Van Nostrand Reinhold, New York.

Yang, H., D. Yang, Z. Lei, and F. Sun (2008), New analytical derivation of the mean annual water-energy balance equation, *Water Resour. Res.*, *44*, W03410, doi:10.1029/2007WR006135.

Yokoo, Y., M. Sivapalan, and T. Oki (2008), Investigating the roles of climate seasonality and landscape characteristics on mean annual and monthly water balances, *J. Hydrol.*, *357*(3–4), 255–269.

Zhang, L., W. R. Dawes, and G. R. Walker (2001), Response of mean annual evapotranspiration to vegetation changes at catchment scale, *Water Resour. Res.*, *37*(3), 701–708.

Zhang, L., K. Hickel, W. R. Dawes, F. H. S. Chiew, A. W. Western, and P. R. Briggs (2004), A rational function approach for estimating mean annual evapotranspiration, *Water Resour. Res.*, *40*, W02502, doi:10.1029/2003WR002710.

X. Feng, A. Porporato, and G. Vico, Department of Civil and Environmental Engineering, 121 Hudson Hall, PO Box 90287, Duke University, Durham, NC 27708-0287, USA. (amilcare.porporato@duke.edu)